



# Hyperlipidaemia elicits an atypical, T helper 1-like CD4<sup>+</sup> T-cell response: a key role for very low-density lipoprotein

**Bram W. van Os** <sup>1</sup>, **Winnie G. Vos**<sup>1</sup>, **Laura A. Bosmans**<sup>1</sup>, **Claudia M. van Tiel**<sup>1</sup>, **Sanne C. Lith**<sup>1</sup>, **Myrthe S. den Toom**<sup>1</sup>, **Linda Beckers**<sup>1</sup>, **Johannes H.M. Levels**<sup>2</sup>, **Suzanne A.E. van Wouw**<sup>1</sup>, **Noam Zelcer**<sup>1</sup>, **Esther A. Zaal**<sup>4</sup>, **Celia R. Berkers**<sup>3,4</sup>, **Chris H.A. van der Lest**<sup>4</sup>, **J. Bernd Helms**<sup>4</sup>, **Christian Weber** <sup>5,6,7,8</sup>, **Dorothee Atzler**<sup>5,6,9</sup>, **Menno P.J. de Winther**<sup>1</sup>, **Jeroen Baardman**<sup>1,†</sup>, and **Esther Lutgens**<sup>1,5,6,10,\*†</sup>

<sup>1</sup>Department of Medical Biochemistry, Experimental Vascular Biology, Amsterdam Infection and Immunity, Amsterdam Cardiovascular Sciences, Amsterdam UMC, University of Amsterdam, Meibergdreef 9, 1105AZ, Amsterdam, Netherlands; <sup>2</sup>Department of Experimental Vascular Medicine, Amsterdam Cardiovascular Sciences, Amsterdam UMC, University of Amsterdam, Meibergdreef 9, 1105AZ, Amsterdam, Netherlands; <sup>3</sup>Biomolecular Mass Spectrometry and Proteomics, Bijvoet Center for Biomolecular Research, Utrecht Institute for Pharmaceutical Sciences, Utrecht University and Netherlands Proteomics Centre, Padualaan 8, 3584CH, Utrecht, Netherlands; <sup>4</sup>Department of Biomolecular Health Sciences, Division of Cell Biology, Metabolism and Cancer, Faculty of Veterinary Medicine, Utrecht University, Yalelaan 2, 3584CM Utrecht, Netherlands; <sup>5</sup>Institute for Cardiovascular Prevention (IPEK), Ludwig-Maximilians-Universität, Pettenkoferstraße 8a and 9, Munich 80336, Germany; <sup>6</sup>German Centre for Cardiovascular Research (DZHK), partner site Munich Heart Alliance, Pettenkoferstraße 8a and 9, Munich 80336, Germany; <sup>7</sup>Department of Biochemistry, Cardiovascular Research Institute Maastricht (CARIM), Maastricht University, Universiteitssingel 50, Maastricht 6229 ER, Netherlands; <sup>8</sup>Munich Cluster for Systems Neurology (SyNergy), Ludwig Maximilian University of Munich, Feodor-Lynen-Str. 17, 81377 Munich, Germany; <sup>9</sup>Walther-Straub-Institute of Pharmacology and Toxicology, Ludwig-Maximilians-Universität, Goethestraße 33D, Munich 80336, Germany; and <sup>10</sup>Department of Cardiovascular Medicine, Experimental Cardiovascular Immunology Laboratory, Mayo Clinic, 200 First St SW, Rochester, MN 55905, USA

Received 11 January 2023; revised 8 February 2023; accepted 9 February 2023; online publish-ahead-of-print 3 March 2023

Handling Editor: Daniel FJ Ketelhuth

## Aims

Hyperlipidemia and T cell driven inflammation are important drivers of atherosclerosis, the main underlying cause of cardiovascular disease. Here, we detailed the effects of hyperlipidemia on T cells.

## Methods and results

*In vitro*, exposure of human and murine CD4<sup>+</sup> T cells to very low-density lipoprotein (VLDL), but not to low-density lipoprotein (LDL) resulted in upregulation of Th1 associated pathways. VLDL was taken up via a CD36-dependent pathway and resulted in membrane stiffening and a reduction in lipid rafts. To further detail this response *in vivo*, T cells of mice lacking the LDL receptor (LDLR), which develop a strong increase in VLDL cholesterol and triglyceride levels upon high cholesterol feeding were investigated. CD4<sup>+</sup> T cells of hyperlipidemic *Ldlr*<sup>-/-</sup> mice exhibited an increased expression of the C-X-C-chemokine receptor 3 (CXCR3) and produced more interferon- $\gamma$  (IFN- $\gamma$ ). Gene set enrichment analysis identified IFN- $\gamma$ -mediated signaling as the most upregulated pathway in hyperlipidemic T cells. However, the classical Th1 associated transcription factor profile with strong upregulation of *Tbet* and *Il12rb2* was not observed. Hyperlipidemia did not affect levels of the CD4<sup>+</sup> T cell's metabolites involved in glycolysis or other canonical metabolic pathways but enhanced amino acids levels. However, CD4<sup>+</sup> T cells of hyperlipidemic mice showed increased cholesterol accumulation and an increased arachidonic acid (AA) to docosahexaenoic acid (DHA) ratio, which was associated with inflammatory T cell activation.

## Conclusions

Hyperlipidemia, and especially its VLDL component induces an atypical Th1 response in CD4<sup>+</sup> T cells. Underlying mechanisms include CD36 mediated uptake of VLDL, and an altered AA/DHA ratio.

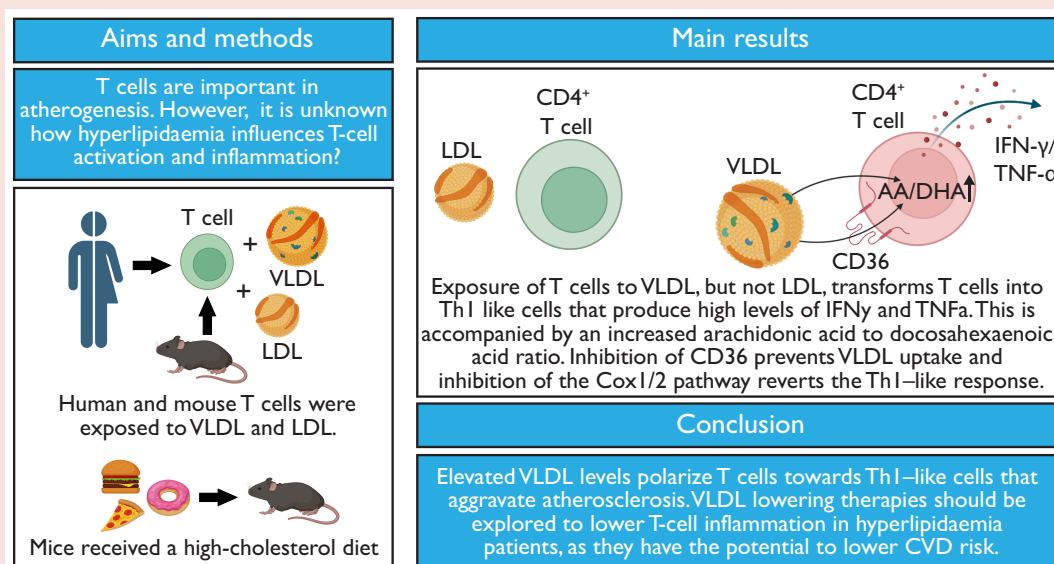
\* Corresponding author. Tel: +1 5075380282, Email: [Lutgens.Esther@mayo.edu](mailto:Lutgens.Esther@mayo.edu)

† These authors contributed equally to the study.

© The Author(s) 2023. Published by Oxford University Press on behalf of the European Society of Cardiology.

This is an Open Access article distributed under the terms of the Creative Commons Attribution-NonCommercial License (<https://creativecommons.org/licenses/by-nc/4.0/>), which permits non-commercial re-use, distribution, and reproduction in any medium, provided the original work is properly cited. For commercial re-use, please contact [journals.permissions@oup.com](mailto:journals.permissions@oup.com)

## Graphical Abstract



## Keywords

T cell inflammation • VLDL • Hyperlipidaemia

## Translational perspective

In this study we demonstrate that high levels of very low density lipoprotein (VLDL) but not low density lipoprotein (LDL) induces an inflammatory response in CD4<sup>+</sup> T cells. This response is characterized by increased production of pro-inflammatory cytokines and increased expression of C-X-C motif chemokine receptor 3 (CXCR3). The effect is mediated by the uptake of VLDL by CD36 and subsequent release of arachidonic acid. Currently, the main focus of the management of hyperlipidaemia is limited to lowering of LDL. However, our data suggests that additional lowering of VLDL could reduce residual cardiovascular risk.

## Introduction

Cardiovascular disease (CVD) remains one of the leading causes of mortality and morbidity worldwide.<sup>1</sup> The underlying pathology of most CVD is atherosclerosis, a chronic inflammatory disease that results in build-up of lipid-rich plaques within medium- and large-sized arteries. Atherosclerotic plaques can obstruct luminal blood flow or become unstable and rupture, leading to cardiovascular events, including myocardial infarction and stroke. Lifestyle and pharmacological interventions targeting traditional cardiovascular risk factors, such as hypertension, diabetes, and hyperlipidaemia, reduce the incidence of CVD. For instance, therapy with 3-hydroxy-3-methylglutaryl coenzyme A (HMG-CoA) reductase inhibitors (statins) to lower plasma levels of low-density lipoprotein cholesterol (LDL-C) results in a decline of cardiovascular events by 25–40%.<sup>2</sup> Despite such gains, cardiovascular events continue to occur at alarming rates in the population, even among patients with controlled LDL-C levels, indicating that other mediators drive the progression of atherosclerosis in these individuals.

In addition to hyperlipidaemia, inflammation is hypothesized to be a crucial driver of atherosclerosis.<sup>3</sup> The *Canakinumab Anti-inflammatory Thrombosis Outcome Study* (CANTOS) trial, where treatment with the anti-interleukin (IL)-1 $\beta$ -neutralizing antibody canakinumab reduces

the rates of cardiovascular events in individuals with elevated C-reactive protein, independent of lipid lowering,<sup>4</sup> has proved that inhibiting inflammation reduces cardiovascular events in humans. Moreover, treatment with colchicine, an inflammasome inhibitor, reduces the risk of recurrent cardiovascular events.<sup>5</sup> However, these treatments had no effect on CVD mortality, and treatment with canakinumab resulted in a slightly higher incidence of infections. Usage of the broad-spectrum anti-inflammatory drug methotrexate failed to significantly reduce cardiovascular events in the *Cardiovascular Inflammation Reduction Trial* (CIRT).<sup>6</sup> Therefore, more tailored immunotherapeutic approaches are needed that effectively fine-tune the complex inflammatory processes in atherosclerosis to prevent cardiovascular events.<sup>7</sup>

Recent mass cytometry and single-cell RNA sequencing analyses revealed that T cells are the most abundant population of leukocytes in human atherosclerotic plaques.<sup>8,9</sup> Numerous data demonstrate that inflammatory T cell responses are a critical player of the development of atherosclerosis.<sup>10</sup> A deeper understanding of the mechanisms that drive pro-atherogenic T cell responses is warranted to develop potential immunotherapeutic strategies to combat CVD. Hyperlipidaemia was previously found to enhance the frequency of effector (memory) T cells in humans and mice.<sup>11–13</sup> Here, we demonstrate that hyperlipidaemia elicits an inflammatory, atypical T helper 1 (Th1) response and

show that this effect is completely reversible upon lipid lowering. Moreover, we show that very low-density lipoprotein (VLDL), and not LDL, is responsible for this inflammatory T cell phenotype.

## Methods

### Mice

C57BL/6J mice deficient for the LDL receptor (*Ldlr*<sup>-/-</sup>) were obtained from Jackson Laboratories. At the age of 10 weeks, male *Ldlr*<sup>-/-</sup> mice were fed a NCD or a 0.15% HCD (Altromin Spezialfutter, 0.15% cholesterol, 15.9% fat, 17.6% protein) for 14 weeks. A third experimental group of *Ldlr*<sup>-/-</sup> mice were fed a HCD for 6 weeks before switching to a NCD (Teklad Global, 0% cholesterol, 4% fat, and 16.4% protein) for another 8 weeks (DS group). Mice were sacrificed by CO<sub>2</sub> asphyxiation, and the heart, blood, spleen, and mesenteric lymph nodes were collected. For *in vitro* experiments, splenocytes obtained from 14- to 22-week-old NCD-fed male *Ldlr*<sup>-/-</sup> mice were used. Animals were housed within the Animal Research Institute AMC (ARIA) with access to water and food *ad libitum*. All animal experiments were performed after approval by the Committee on Animal Welfare of the University of Amsterdam (AVD1180020171666) and conform to the guidelines from Directive 2010/63/EU of the European Parliament on the protection of animals used for scientific purposes.

### LDL and VLDL exposure

Single-cell suspensions were prepared from 16-week-old male *Ldlr*<sup>-/-</sup> mice as described above. Human T cells were isolated from buffy coats from healthy donors acquired from Sanquin Blood Supply (Amsterdam, the Netherlands). Written informed consent was obtained prior to donation in accordance to the principles outlined in the Declaration of Helsinki. Peripheral blood mononuclear cells were isolated using Lymphoprep (Axis-Shield) and subsequent isolation of the complete CD4<sup>+</sup> cell population using CD4<sup>+</sup> beads (Miltenyi Biotec) following the manufacturers provided protocol. Purity of the CD4<sup>+</sup> cell population was assessed by flow cytometry to be a minimum of 95%. Next, cells were cultured in RPMI 1640 medium with HEPES (Thermo Fisher Scientific) supplemented with 10% foetal calf serum (Gibco), penicillin–streptomycin (Gibco), 50 µM 2-mercaptoethanol (Sigma), and 20 ng/mL IL-2 (R&D Systems). Cells were activated by adding anti-CD3/CD28 beads (Thermo Fisher Scientific) in a 1:1 cell-to-bead ratio and exposed to either 5 µg/mL LDL (STEMCELL Technologies) or 5 µg/mL VLDL (Sigma) for 72 h. Cells were lysed in lysis buffer (Qiagen), and material was stored at -80°C prior further processing. Lipoprotein solutions were confirmed to be pure (Table 1).

### Lipid raft and membrane fluidity

Membrane fluidity of CD4<sup>+</sup> T cells was measured with a membrane fluidity kit (Abcam; ab189819) that uses the pyrenedecanoic acid (PDA) monomer-to-excimer ratio to determine membrane fluidity. Fluorescence was measured with a CLARIOstar Plus (BMG Labtech) with excitation set to 350 nm and emissions at 400 nm (monomer)

and 470 nm (excimer). Blanks were subtracted, and the excimer-to-monomer fluorescence ratio was calculated (470 nm/400 nm).

After VLDL treatment, lipid raft was stained with Vybrant Lipid Raft Labeling Kit (Thermo Fisher Scientific, V34404) following the manufacturer's provided protocol. In short, cells were incubated with αCD4 (1:100, APC, BioLegend, #100516) and fixed on coverslips with 4% paraformaldehyde (PFA). To visualize the nucleus, cells were incubated for 15 min with DAPI (Thermo Fisher Scientific, D21490). The coverslips were mounted on slides with MOWIOL (Sigma-Aldrich) and stored in the dark until imaging. Fluorescence images were acquired using the Leica SP8-X confocal microscope (Leica Microsystems). Fluorescence microscopy data were processed and analysed using Icy Software (Institut Pasteur).

### CD4<sup>+</sup> dil-VLDL uptake

Murine CD4<sup>+</sup> T cells were obtained from 16-week-old male *Ldlr*<sup>-/-</sup> as described above.  $2 \times 10^6$  cells were plated in a six-well plate. Prior to VLDL exposure, cells were activated with 50 ng/mL phorbol 12-myristate 13-acetate (PMA; Sigma-Aldrich) and were either incubated with αCD36 (BD Pharmingen, 50 µg/mL, 552 544) or isotype control (BD Pharmingen, 50 µg/mL, 553 476) for 30 min. Medium was supplemented with 50 µg/mL dil-VLDL (Biotrend). Cells were fixed and stained as described previously.

### Histology

After isolation, hearts were fixed with 1% PFA and embedded in paraffin. Hearts were cut in 4 µm sections starting at the appearance of aortic valves and for as long as valves stayed intact. With 24 µm between each section, four serial sections were stained with haematoxylin and eosin to visualize plaques. Plaque area was measured using photoshop software (Adobe), and surface area of the serial sections was plotted in GraphPad Prism software (GraphPad Software). GraphPad was used to calculate the area under the curve to calculate the plaque volume per mouse.

### Blood lipid profile

Blood was obtained by cardiac puncture and collected into tubes containing ethylenediaminetetraacetic acid (EDTA). Lipoprotein, cholesterol, and TG profiles were determined by fast-performance liquid chromatography (FPLC) as described previously.<sup>53</sup> In short, total cholesterol and total TG were measured per major lipoprotein fraction. High-density lipoprotein (HDL), LDL, and VLDL fractions were separated on an FPLC comprised a PU-980 ternary pump and an LG-980-02 linear degasser with an UV-975 UV/VIS detector (JASCO). After injection of 30 µL plasma, diluted with 1:1 with Tris-buffered saline (TBS), lipoproteins were separated using a Superose 6 increase 10/30 column (GE Healthcare). Tris-buffered saline (pH 7.4) was used an eluent at a flow rate of 0.31 mL/min. For in-line measurement of cholesterol PAP or TG enzymatic substrate reagent (Sopachem), a second pump was used (PU-2080i Plus, JASCO) at a flow rate of 0.1 mL/min for total cholesterol and total TG detection. To aid in the quantification of cholesterol and TG, commercially available lipid plasma standards were used to generate calibration curves. All calculations performed on the chromatograms were carried out with ChromNAV chromatographic software, version 1.0 (JASCO).

### Flow cytometry

For the examination of surface markers on T cells from blood, lymph nodes, and spleen, single-cell suspensions were prepared by meshing harvested spleens and lymph nodes through a 70 µm cell strainer

**Table 1** Composition of lipoprotein solutions used in *in vitro* experiments

|          | LDL         | VLDL       |
|----------|-------------|------------|
| ApoA-I   | 0.82 mg/dL  | 0.54 mg/dL |
| ApoB-48  | 0.7 mg/dL   | 8.1 mg/dL  |
| ApoB-100 | 54.86 mg/dL | 56.4 mg/dL |

(Corning). Erythrocytes were lysed in buffer containing 150 mM ammonium chloride and 10 mM sodium bicarbonate (pH 7.4).

For the identification of CD36<sup>+</sup> T cell and naïve/effector subpopulations, the following antibodies were used:  $\alpha$ CD16/CD32 (1:1000, BioLegend, #101330),  $\alpha$ CD3e (1:200, BV510, BioLegend, #100353),  $\alpha$ CD4 (1:400, Pacific Blue, BioLegend, #100427),  $\alpha$ CD8a (1:400, APC-Cy7, BioLegend, #100713),  $\alpha$ CD36 (1:100, Alexa Fluor 488, Bio-Rad, MCA2748),  $\alpha$ CD44 (1:800, APC, BioLegend, #103012), and  $\alpha$ CD62L (1:1000, PE-Cy7, #104418). Prior to analysis, 7-AAD (1:1000, Thermo Fisher Scientific, #A1310) was added to exclude dead cells.

To identify T cell subsets based on chemokine receptor, expression samples were incubated with the following antibodies in FACS  $\alpha$ CD16/CD32 (1:1000, BioLegend, #101330),  $\alpha$ CD3e (1:200, BV510, BioLegend, #100353),  $\alpha$ CD4 (1:400, Pacific Blue, BioLegend, #100427),  $\alpha$ CD8a (1:400, APC-Cy7, BioLegend, #100713),  $\alpha$ CCR4 (1:100, PE, BioLegend, 101 203),  $\alpha$ CCR6 (1:100, BV605, BioLegend, 129 819), and  $\alpha$ CXCR3 (1:100, BUV563, BD Biosciences, 741 438). Prior to analysis, 7-AAD (1:1000, Thermo Fisher Scientific, #A1310) was added to exclude dead cells.

For the detection of intracellular cytokines, splenocytes or human PBMCs were exposed to 50 ng/mL phorbol 12-myristate 13-acetate (PMA; Sigma-Aldrich) and 1  $\mu$ M ionomycin (Sigma-Aldrich) for 5 h. Monensin (Thermo Fisher Scientific) and brefeldin A (Qiagen) were added after 1 h. Afterwards, cells stained with Fixable Near-IR Live/Dead (Thermo Fisher Scientific) diluted 1:1000 in phosphate-buffered saline (PBS) for 30 min on ice.

The murine cells were stained within FACS buffer with the following antibodies:  $\alpha$ CD16/CD32 (1:1000, BioLegend, #101330),  $\alpha$ CD3e (1:400, APC, BioLegend, #100312),  $\alpha$ CD4 (1:400, Pacific Blue, BioLegend, #100427), and  $\alpha$ CD8a (1:800, FITC, Thermo Fisher Scientific, #11-0081). Next, cells were fixed, permeabilized, and stained using the Foxp3/Transcription Factor Staining Buffer Set (Thermo Fisher Scientific) according to the manufacturer's provided protocol. Cells were stained for the presence of cytokines in permeabilization buffer with the following antibodies:  $\alpha$ IL-4 (1:200, PE, BioLegend, #504104),  $\alpha$ IL-17A (1:200, BUV395, BD Biosciences, #565246), and  $\alpha$ IFN- $\gamma$  (1:800, BV785, BioLegend, #505838). Human cells were incubated with the following antibodies: Human TruStain FcX (1:1000, BioLegend, #422302),  $\alpha$ CD4 (1:200, BV421, BioLegend, #317433), and  $\alpha$ CD8a (1:200, PE-Cy7, BioLegend, #344712). Cells were fixed and permeabilized as described above and incubated with  $\alpha$ TNF- $\alpha$  (1:100, PE, BioLegend, #502909) and  $\alpha$ IFN- $\gamma$  (1:200, BV786, BioLegend, #502541).

Samples were measured on a LSRFortessa or Symphony A1 Cell Analyzer (BD Biosciences) and analysed using FCS Express software, version 7 (De Novo Software).

## Fluorescence-activated cell sorting

Single-cell suspensions were prepared by meshing harvested spleens through a 70  $\mu$ m cell strainer (Corning). Erythrocytes were lysed in buffer containing 150 mM ammonium chloride and 10 mM sodium bicarbonate (pH 7.4) for 5 min on ice, and samples were washed with PBS. All cells were first stained in FACS buffer with  $\alpha$ CD16/CD32 (1:1000, BioLegend, #101330) for 10 min on ice. Subsequently, cells were stained with  $\alpha$ CD3e (1:400, FITC, Thermo Fisher Scientific, #11-0031-82),  $\alpha$ CD4 (1:800, PE, Thermo Fisher Scientific, #12-0041-82),  $\alpha$ CD8a (1:400, APC-Cy7, BioLegend, #100713),  $\alpha$ CD19 (1:400, PE-Cy7, BioLegend, #115519), and  $\alpha$ CD25 (1:800, APC, Thermo Fisher Scientific, #17-0251-82). Prior to sorting, 7-AAD (1:1000, Thermo Fisher Scientific, #A1310) was added to exclude dead cells. Cell population were sorted using a FACSAria II (BD Biosciences).

## Transcriptomics

Sorted cells were washed with ice-cold PBS and lysed in RLT buffer, and total RNA was isolated using the RNeasy Mini Kit with an on-column DNase treatment according to the manufacturer's instructions (Qiagen). RNA concentration was determined using a Qubit fluorometer (Qiagen), while RNA quality was evaluated using an Agilent Bioanalyzer 2100 system (Agilent Technologies) prior to strand-specific library preparation using the KAPA mRNA HyperPrep Kit according to the manufacturer's instructions. Libraries were pooled and diluted to 25 nM prior to sequencing on a HiSeq 4000 instrument (Illumina) for the hyperlipidaemia experiment or on a NovaSeq 6000 (Illumina) for the *in vitro* mouse and human experiment, both at a depth of 20 million single-ended 50 base pair reads. Reads were aligned to the mouse genome mm10 using STAR 2.5.2b with default settings.<sup>54</sup> BAM files were indexed and filtered on MAPQ > 15 with SAMtools 1.3.1.<sup>55</sup> Raw tag counts and reads per kilobase per million mapped reads (RPKM) values per gene were summed using HOMER2's analyzeRepeats.pl script with default settings and the -noadj or -rpkm options for raw counts and RPKM reporting, respectively. Differential expression was assessed using the DESeq2 Bioconductor package in an R 4.1.1 environment with a Benjamini–Hochberg adjusted *P* value < 0.05 and an average RPKM > 1 in at least one group.<sup>56</sup> Human samples were analysed pairwise. To identify deregulated pathways, GSEA was performed using the clusterProfiler Bioconductor package.<sup>57</sup> Pathway enrichment analysis was performed using Metascape.<sup>58</sup> Differentially up-regulated and down-regulated genes were analysed separately to assess enriched down-regulated and up-regulated gene sets. Only gene sets with a minimum of 10 genes and enrichment of 5 genes were included in the analysis. Pscan was applied to detect over-represented TF-binding site motifs.<sup>59</sup> Volcano plots and heatmaps were generated in an R 4.1.1 environment using the ggplot2 and pheatmap packages, respectively.<sup>60,61</sup>

## Metabolomics

Sorted cells were washed with ice-cold PBS, and metabolites were extracted in 50  $\mu$ L lysis buffer containing methanol/acetonitrile/dH<sub>2</sub>O (2:2:1). Samples were centrifuged at 16,000 g for 15 min at 4°C to remove cell debris and proteins, and supernatants were collected for LC–MS analysis. Liquid chromatography with mass spectrometry analysis was performed on a Q-Exactive HF mass spectrometer (Thermo Fisher Scientific) coupled to a Vanquish autosampler and pump (Thermo Fisher Scientific). The MS operated in polarity-switching mode with spray voltages of 4.5 and –3.5 kV. Metabolites were separated using a SeQuant ZIC-pHILIC column (2.1  $\times$  150 mm, 5  $\mu$ m, guard column 2.1  $\times$  20 mm, 5  $\mu$ m; Merck) with elution buffers acetonitrile (A) and eluent B [20 mM (NH<sub>4</sub>)<sub>2</sub>CO<sub>3</sub>, 0.1% NH<sub>4</sub>OH in ULC–MS grade water (Biosolve)]. Gradient ran from 20% eluent B to 60% eluent B in 20 min, followed by a wash step at 80% and equilibration at 20%. Flow rate was set at 100  $\mu$ L/min. Analysis was performed using TraceFinder software (Thermo Fisher Scientific). Metabolites were identified and quantified based on exact mass within 5 ppm and further validated by concordance with retention times of standards. Peak intensities were normalized based on total intensity.

## Lipidomics

Lipids were extracted using the method described by Bligh and Dyer.<sup>62</sup> Lipid extracts were dried under N<sub>2</sub>, dissolved in 100  $\mu$ L of chloroform and methanol (1:1), and injected (10  $\mu$ L) into a hydrophilic interaction liquid chromatography column (2.6  $\mu$ m HILIC 100 Å, 50  $\times$  4.6 mm, Phenomenex). Lipid classes were separated by gradient elution on an Infinity II 1290 UPLC (Agilent) at a flow rate of 1 mL/min. A mixture of acetonitrile and acetone (9:1, v/v) was used as solvent A, while solvent B consisted of a mixture of acetonitrile, H<sub>2</sub>O (7:3, v/v) with 50 mM ammonium formate. Both A and B contained 0.1% formic acid (v/v).



Gradient elution was done as follows (time in min, % B): (0, 0), (1, 50), (3, 50), (3.1, 100), and (4, 100). No re-equilibration of the column was necessary between successive samples. The column effluent was connected to a heated electrospray ionization (hESI) source of an Orbitrap Fusion mass spectrometer (Thermo Fisher Scientific) operated at  $-3600$  V in the negative ionization mode. The vaporizer and ion transfer tube were set at a temperature of  $275^{\circ}\text{C}$  and  $380^{\circ}\text{C}$ , respectively. Full scan measurements (MS1) in the mass range from 450 to 1150 amu were collected at a resolution of 120 000. Parallelized data-dependent MS2 experiments were done with HCD fragmentation set at 30 V, using the dual-stage linear ion trap to generate up to 30 spectra per second.

The dried neutral lipids were dissolved in a mixture of chloroform and methanol (1/1; v/v). The lipids were separated on a HALO C8 fused-core column ( $3.0 \times 150$  mm,  $2.7 \mu\text{m}$ ; Advanced Materials Tech) using a gradient from 25% to 100% methanol/2-propanol (8/2; v/v) in methanol/water (1/1; v/v) in 1 min and an additional 13 min elution with methanol/2-propanol. Elution was at  $40^{\circ}\text{C}$  and a flow rate of  $300 \mu\text{L}/\text{min}$ . The column effluent was connected to an atmospheric pressure chemical ionization (APCI) source attached to a Q-Exactive HF mass spectrometer. Full scan measurements (MS1) in the mass range from 450 to 1150 amu were collected at a resolution of 120 000.

The phospholipid and neutral lipid LC-MS data were processed using an R-script based on the package 'XCMS' for peak recognition and integration.<sup>63</sup> Lipid classes were identified based on retention time, and molecular species were then matched against an *in silico* generated lipid database. This database was constructed based on theoretical fatty acyls combined with the lipid head group structure. Mass accuracy of annotated lipids was typically below 2 ppm.

## Ibuprofen

CD4<sup>+</sup> cells were harvested and exposed to LDL and VLDL as described previously. Before LDL or VLDL exposure, cells were pre-incubated with 1 mM ibuprofen (Sigma-Aldrich) for 30 min. Lipoprotein suspensions were added and medium containing fresh ibuprofen and either LDL or VLDL every day. After 4 days, cytokine production was assessed by intracellular cytokine staining as described previously.

## Statistical analysis

Statistical analyses were performed using GraphPad Prism software version 9 (GraphPad Software Inc.). Data in bar graphs are presented as mean  $\pm$  standard deviation (SD). A Shapiro–Wilk test was applied to test for normality. For normally distributed data, statistical significance between the three diet groups was analysed using an ordinary one-way analysis of variance (ANOVA) followed by a Tukey's multiple comparison test. A Kruskal–Wallis test with a subsequent Dunn's multiple comparison test was used to assess significance between the groups for data not following a Gaussian distribution. *P* values  $< 0.05$  were considered statistically significant. Levels of significance are indicated as follows: \**P*  $< 0.05$ , \*\**P*  $< 0.01$ , and \*\*\**P*  $< 0.001$ .

## Results

### VLDL, but not LDL, elicits an inflammatory response in human and mouse CD4<sup>+</sup> T cells *in vitro*

Since hyperlipidaemia is characterized by elevated levels of plasma lipoproteins, we first assessed the effect of LDL and VLDL on T cell activation. Hereto, we exposed CD3/CD28 bead-activated human CD4<sup>+</sup> T cells to either LDL or VLDL. Exposure to LDL did not alter the transcriptome of T cells, as no genes were detected to be differentially expressed (adjusted *P* value  $< 0.05$ ) between cells incubated with or without LDL (Figure 1A).

In contrast, upon exposure to VLDL, 12 differentially expressed genes (DEGs) were identified (Figure 1B). Gene set enrichment analysis (GSEA) identified the TNFR2 non-canonical nuclear factor kappa B (NF- $\kappa$ B) pathway as the most significant enriched gene set in T cells upon treatment with VLDL (Figure 1C). Moreover, we found an enrichment of processes involved in immune cell activation and immune effector responses (Figure 1C). Very low-density lipoprotein treatment also resulted in an array of down-regulated genes and pathways, mostly associated with cell cycle, chromatin organization, and apoptosis (Figure 1C). These pathways are all connected, as after activation T cells proliferate, polarize, and exert their actions after which they go into apoptosis.

In addition to this enhanced pro-inflammatory response at the level of transcription, T cells exposed to VLDL demonstrated elevated cytokine production of tumour necrosis factor- $\alpha$  (TNF- $\alpha$ ) (Figure 1D). This cytokine is associated with the pro-inflammatory Th1 subset of CD4<sup>+</sup> T cells. In contrast, levels of the signature Th1 cytokine interferon- $\gamma$  (IFN- $\gamma$ ) remained unaltered upon VLDL exposure.

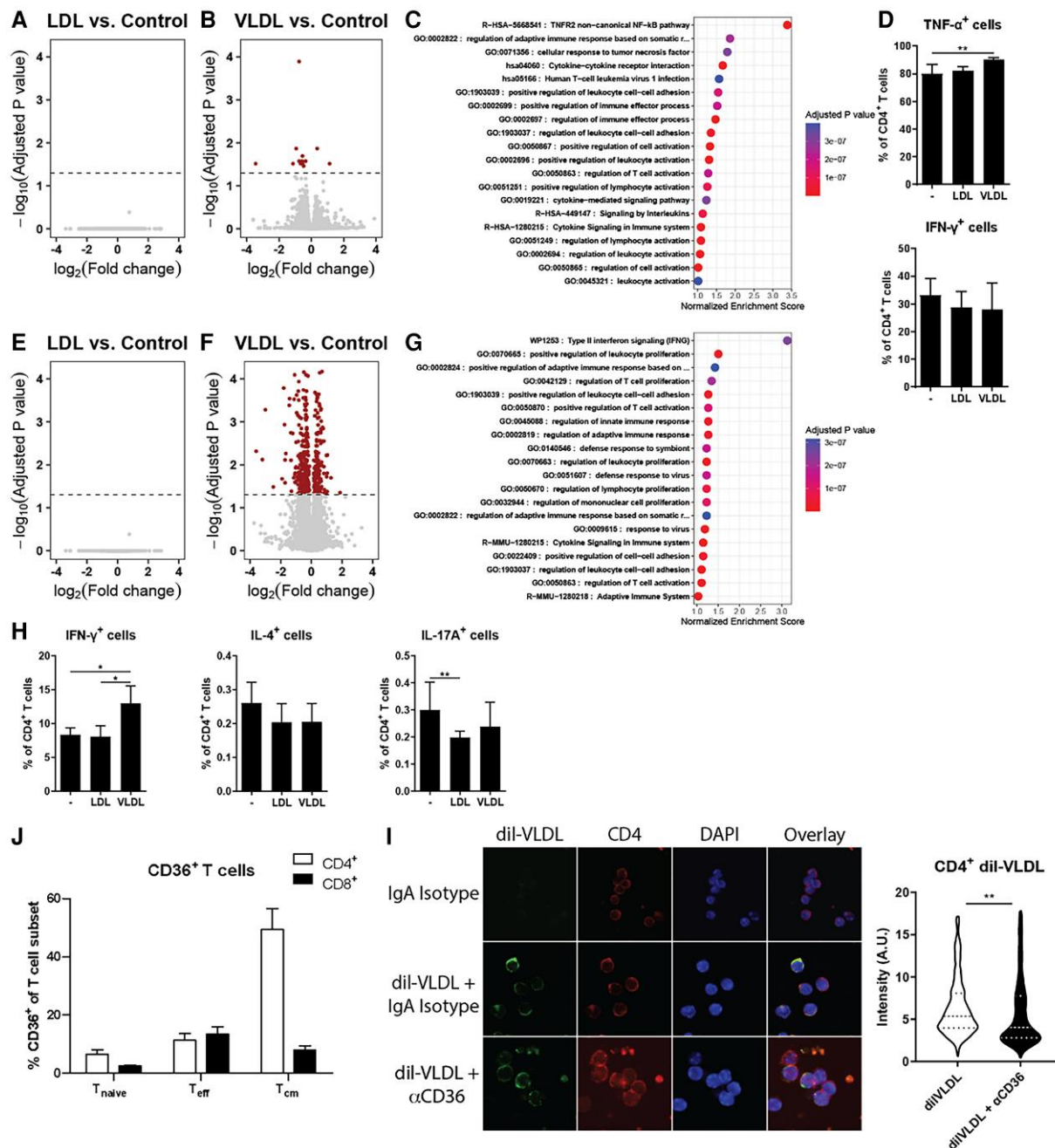
In a similar experiment conducted in murine T cells, exposure to LDL again did not alter the transcriptome of T cells (Figure 1E), whereas exposure to VLDL had a pronounced impact on the transcriptomic profile of T cells, with 523 genes found to be differentially expressed (Figure 1F). Gene set enrichment analysis identified IFN- $\gamma$  signalling as the most enriched gene set in T cells upon exposure to VLDL (Figure 1G). Likewise, exposure to VLDL resulted in enhanced cytokine production of IFN- $\gamma$  (Figure 1H).

Confocal imaging of dil-VLDL-exposed CD4<sup>+</sup> T cells showed that VLDL particles are being taken up by CD4<sup>+</sup> T cells. The most common receptors that facilitate VLDL uptake in hepatocytes and macrophages are the VLDL receptor (VLDL-R) and, to a lesser extent, LDL receptor-related protein 1 (LRP1).<sup>14,15</sup> However, our transcriptomic data show that VLDL-R and LRP1 are not detectable on T cells. Alternative receptors that can take up VLDL are two members of the SR-B family: SR-B1 and CD36. CD36 is present on T cells and is predominantly expressed on CD4<sup>+</sup> effector and memory T cells (Figure 1I). Antibody-mediated inhibition of CD36 receptor significantly lowered the amount of VLDL uptake (Figure 1J), suggesting that CD36, at least partially, mediates VLDL uptake in T cells. Altogether, these findings indicate that VLDL, and not LDL, elicits an inflammatory response in both human and murine CD4<sup>+</sup> T cells.

### Hyperlipidaemia results in an increase of effector CD4<sup>+</sup> T cells *in vivo*

To further detail this response *in vivo*, LDL receptor knockout (*Ldlr*<sup>-/-</sup>) mice, which are well known for their high VLDL levels upon high-cholesterol feeding, were used and randomized into three groups. The first group was fed a normal chow diet (NCD). The second and third groups were fed a 0.15% high-cholesterol diet (HCD). The third group received a HCD for 6 weeks and was then switched to a NCD for another 8 weeks [diet-switch (DS) group]. As a control for the DS group, mice were fed a HCD for 6 weeks (6-week HCD) (Figure 2A). As expected, *Ldlr*<sup>-/-</sup> mice fed a HCD developed profound hypercholesterolaemia and hypertriglyceridaemia (Figure 2B and C). The HCD-induced increase of cholesterol was limited to VLDL and LDL particles, whereas the raise of triglyceride (TG) was restricted to the VLDL fraction (Figure 2D and E). However, switching these mice after 6 weeks of HCD to a NCD completely normalized plasma cholesterol and TG levels (Figure 2B–E). Accordingly, atherosclerotic plaque area had significantly increased in mice from the HCD group, and withdrawal of the diet (DS) resulted in similar plaque burden as observed in mice fed a NCD (Figure 2F).

Next, we assessed whether these diet-induced changes in plasma lipid levels affected T cell numbers and subset composition. In spleen, HCD feeding did not affect CD3<sup>+</sup> T cell numbers (NCD:  $31.01 \pm 2.86\%$ ; HCD:  $31.03 \pm 3.69\%$ ; DS:  $30.88 \pm 2.32\%$ , data not shown)



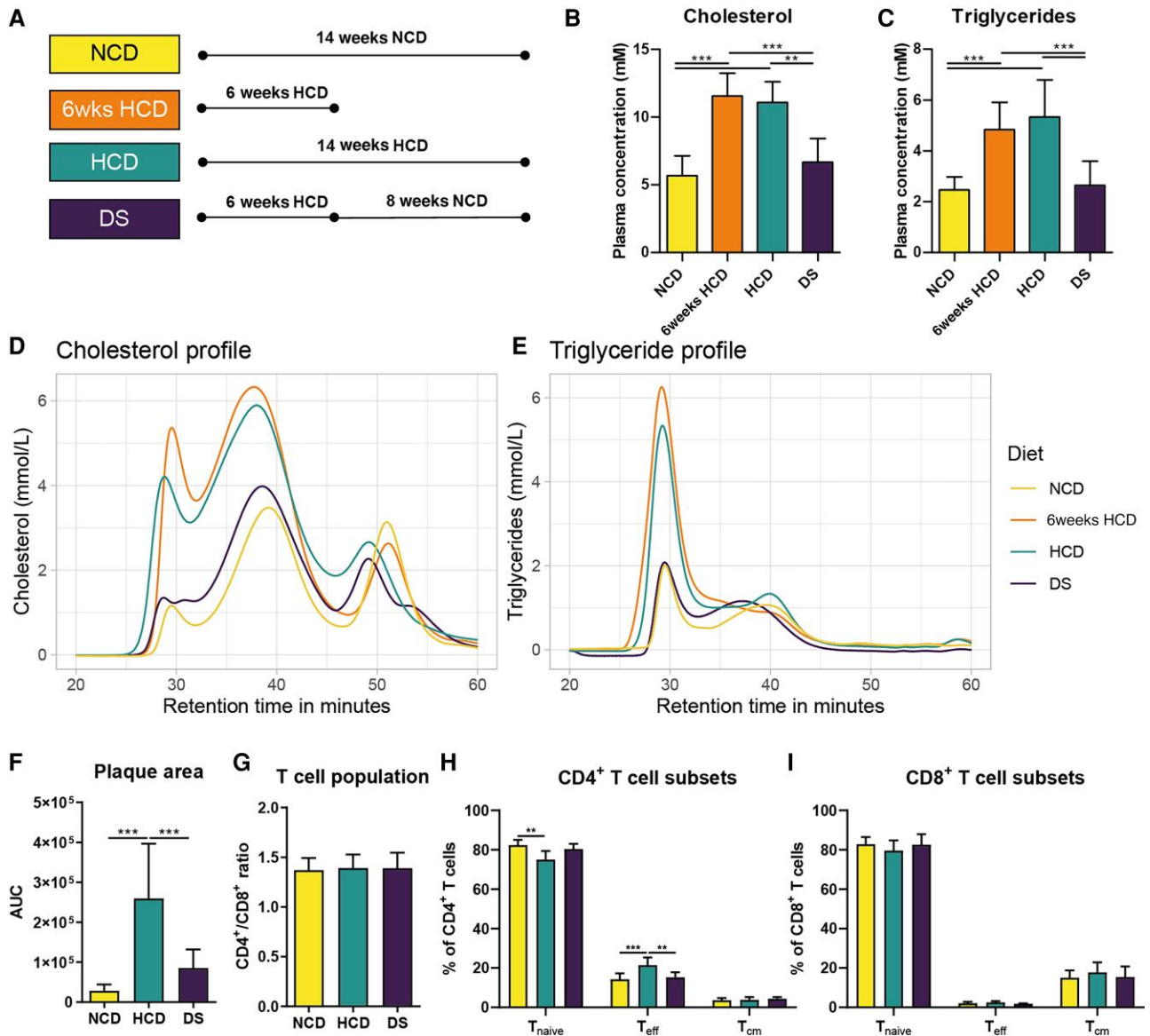


**Figure 2** (A) Experimental design of the *Ldlr*<sup>-/-</sup> mouse study. (B) Total cholesterol ( $n = 13$  NCD,  $n = 14$  HCD,  $n = 13$  DS) and (C) TG levels ( $n = 11$  NCD,  $n = 12$  6-week HCD,  $n = 14$  HCD,  $n = 13$  DS) in plasma. (D and E) Representative cholesterol and triglyceride plasma profiles for each experimental group. (F) Quantification of the atherosclerotic plaque size ( $n = 9$  NCD,  $n = 9$  HCD,  $n = 9$  DS). (G) Ratio of CD4<sup>+</sup> and CD8<sup>+</sup> T cells in the spleen ( $n = 9$  NCD,  $n = 7$  HCD,  $n = 8$  DS). (H and I) Percentage of naïve (CD44<sup>+</sup>CD62L<sup>+</sup>), effector (CD44<sup>+</sup>CD62L<sup>-</sup>), and central memory (CD44<sup>+</sup>CD62L<sup>+</sup>) cells within the splenic (H) CD4<sup>+</sup> ( $n = 9$  NCD,  $n = 7$  HCD,  $n = 8$  DS) and (I) and CD8<sup>+</sup> ( $n = 9$  NCD,  $n = 6/7$  HCD,  $n = 8$  DS) T cell population. Data are shown as mean  $\pm$  SD. Statistical significance was analysed by first removing outliers using a ROUT test. Normal distribution of the data was determined by a Shapiro–Wilk normality test. Non-normally distributed data was analysed column wise by Kruskal–Wallis ranked tests followed, by Dunn’s multiple comparisons test. (B) Normally distributed data were analysed by a one-way ANOVA, followed by Tukey’s multiple comparison test (C and F–I). Statistical significance is displayed as \* $P < 0.05$ , \*\* $P < 0.01$ , and \*\*\* $P < 0.001$ .

or the CD4<sup>+</sup>/CD8<sup>+</sup> T cell ratio (Figure 2G). However, HCD feeding increased the fraction of splenic effector CD4<sup>+</sup> T cells, which was restored in the DS group after switching the diet to a NCD (Figure 2H). In the CD8<sup>+</sup> population, numbers of naïve, effector, and central memory T cells remained unaffected (Figure 2I). High-cholesterol diet induced an increase in the number of regulatory T cells (Tregs), which remained high after switching the HCD to a NCD

(see Supplementary material online, Figure S1A). Similar results were found in mesenteric lymph nodes (see Supplementary material online, Figure S1B). Together, these results indicate that CD4<sup>+</sup> T cells acquire an effector phenotype upon diet-induced hyperlipidaemia, which is in line with our *in vitro* data (Figure 1). Interestingly, this increased activated T cell state could be fully reversed upon DS, when plasma lipid levels are normalized.



## Hyperlipidaemia enhances interferon signalling in CD4<sup>+</sup> T cells

To examine the effects of a hyperlipidaemic environment on T cells in more detail, we isolated splenic CD4<sup>+</sup> T cells and CD8<sup>+</sup> T cells from mice of the three diet groups and performed RNA-seq analysis. Principal component analysis (PCA) showed that the NCD/DS and HCD groups were clearly separated in CD4<sup>+</sup> T cells, but not in CD8<sup>+</sup> T cells, suggesting that CD4<sup>+</sup> T cells are more sensitive to hyperlipidaemia than CD8<sup>+</sup> T cells (see [Supplementary material online, Figure S2A](#)). In CD4<sup>+</sup> T cells, we found 27 genes to be differentially expressed between T cells from the NCD and HCD group, with almost all DEGs found to be up-regulated ([Figure 3A and D](#)). When comparing T cells from the HCD and DS group, we identified 20 DEGs, including 13 up-regulated DEGs and seven down-regulated DEGs ([Figure 3B and E](#)). Interestingly, no DEGs were identified between T cells from the NCD and DS group, indicating that the transcriptomic profile of T cells is normalized upon reversal of hyperlipidaemia ([Figure 3C](#)). Pathway analysis in CD8<sup>+</sup> T cells only showed minor changes (see [Supplementary material online, Figure S2B](#)).

Using GSEA, we revealed IFN- $\gamma$  signalling as the most significantly enriched process in CD4<sup>+</sup> T cells from HCD-fed mice ([Figure 3F](#)). In addition, the IFN- $\beta$  response was captured as the second-most enriched gene set upon hyperlipidaemia in T cells. Interferons are effector molecules with strong antiviral and immunomodulatory capacities.<sup>16</sup> Binding of IFNs to specific receptors on the surface of cells results in the activation of Janus kinases and subsequent phosphorylation of signal transducer and activator of transcription (STAT1) and STAT2. Together with IFN regulatory factor 9 (IRF9), STAT1 and STAT2 form the IFN-stimulated gene factor (ISGF)-3 complex that binds to specific elements in IFN-stimulated genes (ISGs) to induce their expression.<sup>16,17</sup> In line with an increased IFN response, transcription factor (TF)-binding motif analysis identified the putative binding site for IRF9 as the most over-represented binding motif for TFs in T cells upon hyperlipidaemia ([Figure 3G](#)). In addition to IRF9, TF-binding sites for other IRFs and STAT1/STAT2 were among the most significantly enriched motifs. Collectively, these results demonstrate that hyperlipidaemia drives CD4<sup>+</sup> T cells towards a more activated state with an enhanced IFN signalling signature.

## CD4<sup>+</sup> T cells under hyperlipidaemic conditions acquire T helper 1-like features but are distinct from T helper 1 cells

Given the importance of autocrine IFN- $\gamma$  signalling for the differentiation of naïve CD4<sup>+</sup> T cells into Th1 cells,<sup>18</sup> we tested whether the observed IFN- $\gamma$  gene signature ([Figure 3F and G](#)) correlated with enhanced Th1 differentiation. Hereto, we measured the surface expression of C-X-C-chemokine receptor 3 (CXCR3), a marker associated with Th1 cells. Compared to the NCD and DS group, we indeed found an expansion of the splenic CD4<sup>+</sup>CXCR3<sup>+</sup> cell population in hyperlipidaemic mice ([Figure 4A](#)). Similar to the results observed in our VLDL-exposed CD4<sup>+</sup> T cells ([Figure 1H](#)), production of the Th1 cytokine IFN- $\gamma$  was significantly enhanced in *ex vivo* stimulated splenic T cells from HCD-fed mice ([Figure 4B](#)), while TNF- $\alpha$  levels remained unaltered (see [Supplementary material online, Figure S3A](#)). The induction of IFN- $\gamma$  was already observed after 6 weeks of HCD feeding (see [Supplementary material online, Figure S3B](#)). No differences in surface expression of C-C chemokine receptor type 4 (CCR4) or production of IL-4, both characteristics of Th2 cells, were observed between the three groups ([Figure 4C and D](#)), and typical Th17 markers CCR6 and IL-17A remained unaffected ([Figure 4E and F](#)). A similar Th1-like phenotype could be observed in CD4<sup>+</sup> T cells obtained from mesenteric lymph nodes (see [Supplementary material](#)

[online, Figure S3C](#)). These observations suggest that hyperlipidaemia induces a Th1 phenotype, without affecting Th2 and Th17 differentiation. We further explored our RNA-seq data to examine the pro-inflammatory Th1 response at the transcriptional level and applied unsupervised hierarchical cluster analysis. However, based on canonical Th1 genes, we were not able to discriminate between T cells among the different groups ([Figure 4G](#)). Thus, while T cells from HCD-fed mice acquire features of Th1 cells, such as up-regulated surface expression of CXCR3 and elevated IFN- $\gamma$  production, their transcriptomic profile is different from a classical Th1 response.

## Hyperlipidaemia induces only minor changes in CD4<sup>+</sup> T-cell metabolism

An increasing number of studies emphasize that metabolic reprogramming of T cells serves as a crucial regulator of their phenotype and function.<sup>19,20</sup> However, T cells isolated from the three groups of mice could not be separated based on genes encoding enzymes involved in canonical metabolic pathways associated with T cell activation, such as the glycolysis, pentose phosphate pathway (PPP), tricarboxylic acid (TCA) cycle, and glutaminolysis (see [Supplementary material online, Figure S4A](#)). Next, we measured the intracellular levels of a set of metabolites in T cells, including amino acids, pyrimidines, purines, carnitines, and intermediates of the glycolysis and TCA cycle using liquid chromatography with mass spectrometry (LC-MS). However, PCA performed on the metabolomics data revealed no clear separation between the groups (see [Supplementary material online, Figure S4B](#)). Together, these observations suggest that hyperlipidaemia is not accompanied by significant remodelling of canonical metabolic pathways related to T cell activation. Nevertheless, levels of the metabolites adenosine, creatine, nicotinamide, nicotinamide adenine dinucleotide phosphate (NAPDH), guanosine monophosphate (GMP), two carnitines, and six amino acids were found to be significantly altered between T cells from NCD- and HCD-fed mice (see [Supplementary material online, Figure S4C](#)). Interestingly, hyperlipidaemia caused enrichment of isoleucine, lysine, methionine, tryptophan, tyrosine, and valine in T cells upon hyperlipidaemia.

## Hyperlipidaemia alters the fatty acid composition of phospholipids in CD4<sup>+</sup> T cells

Given the relationship between cholesterol and T cell activation,<sup>21</sup> and the elevated levels of plasma cholesterol in our experimental model, we examined the expression of canonical genes involved in cholesterol homeostasis in more detail. Remarkably, genes that are required to raise (*Srebf2*, *Hmgcr*, and *Ldlr*) and decrease (*Insig1*, *Abca1*, *Abcg1*, and *Mylip*) intracellular cholesterol content were up-regulated simultaneously in CD4<sup>+</sup> T cells from HCD-fed mice (see [Supplementary material online, Figure S5A](#)), suggesting an increased turnover of cholesterol in cells. To detail the effects of hyperlipidaemia on the lipid profile of CD4<sup>+</sup> T cells, LC-MS-based lipidomics was applied. In total, 132 unique neutral lipids from six lipid classes and 172 unique phospholipids from 10 lipid classes were identified. Based on the total neutral lipid composition in CD4<sup>+</sup> T cells, we were not able to distinguish the different diet groups ([Figure 5A](#)). Moreover, no significant differences in the abundance of neutral lipid classes were observed ([Figure 5B](#)). As T cells are not the main cholesterol handling cell types, as compared to hepatocytes and macrophages, and probably not capable of major changes in the lipid compartment, major shifts in the major cellular lipid classes were not observed. Nevertheless, slightly elevated cholesterol levels were detected in CD4<sup>+</sup> T cells upon hyperlipidaemia (see [Supplementary material online, Figure S5B](#)). In contrast to neutral lipids,



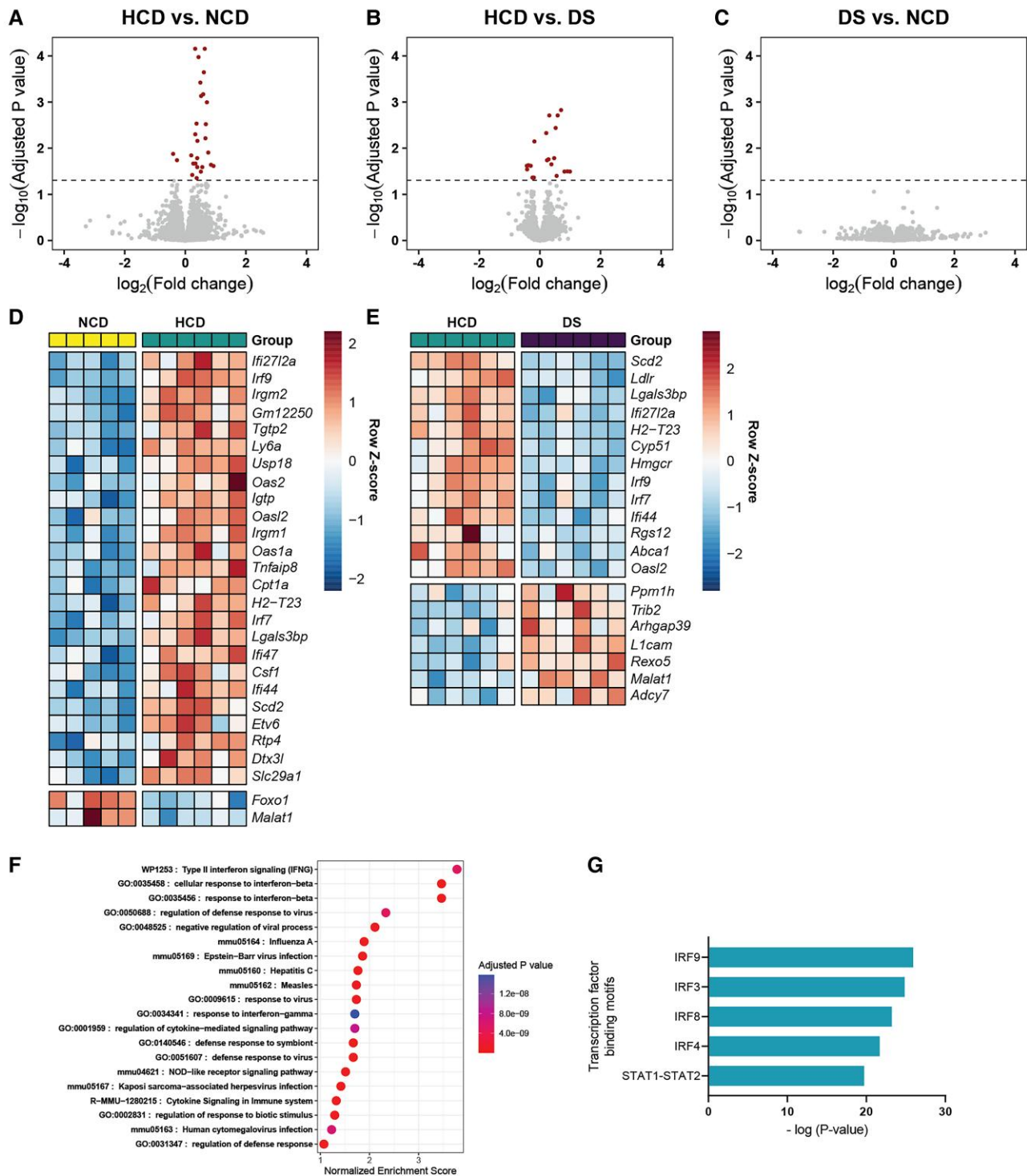


**Figure 3** (A–C) Volcano plots showing the comparison in gene expression between splenic CD4<sup>+</sup> T cells from the different diet groups ( $n = 5$  NCD,  $n = 6$  HCD,  $n = 6$  DS) as determined by RNA-seq. Differentially expressed genes (adjusted  $P < 0.05$ ) are highlighted. (D) Expression heatmaps of the DEGs between (D) HCD vs. NCD and (E) HCD vs. DS splenic CD4<sup>+</sup> T cells. (F) Most enriched gene sets in splenic CD4<sup>+</sup> T cells from hyperlipidaemic mice (NCD vs. HCD) as determined by GSEA. (G) Enrichment plot of the most enriched gene set. (H) Most over-represented binding motif for transcription factors.

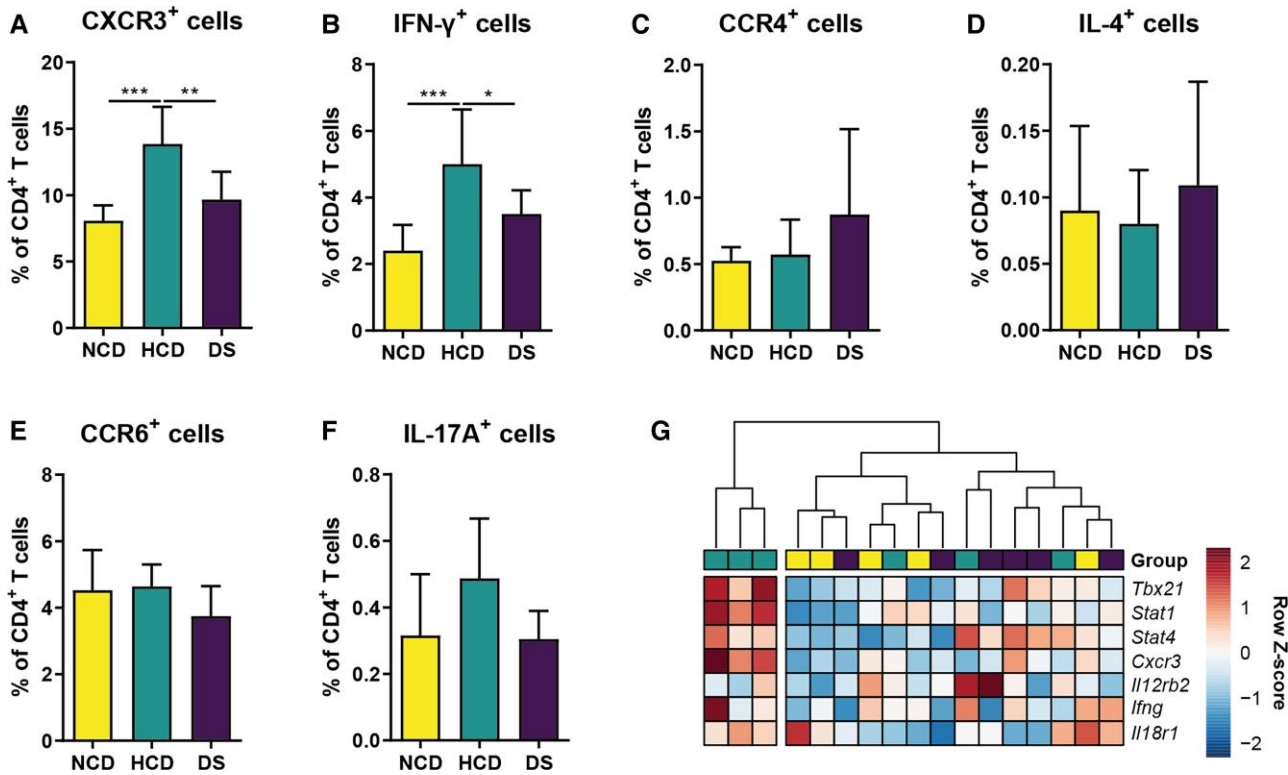


**Figure 4** (A–F) Frequencies of splenic CD4<sup>+</sup> T cells positive for Th1 markers (A) CXCR3 ( $n = 5$  NCD,  $n = 8$  HCD,  $n = 9$  DS) and (B) IFN- $\gamma$  ( $n = 9$  NCD,  $n = 7$  HCD,  $n = 10$  DS), Th2 makers, (C) CCR4 ( $n = 4$  NCD,  $n = 8$  HCD,  $n = 10$  DS), and (D) IL-4 ( $n = 9$  NCD,  $n = 7$  HCD,  $n = 10$  DS) and Th17 markers (E) CCR6 ( $n = 4$  NCD,  $n = 8$  HCD,  $n = 9$  DS) and (F) IL-17A ( $n = 9$  NCD,  $n = 7$  HCD,  $n = 10$  DS) as quantified by flow cytometry. For the measurement of intracellular cytokines (B, D, and F), splenic CD4<sup>+</sup> T cells were first stimulated with PMA and ionomycin. (G) Unsupervised hierarchical clustering of canonical Th1 gene expression. Data are shown as mean  $\pm$  SD. Statistical significance was analysed by first removing outliers using a ROUT test. Normal distribution of the data was determined by a Shapiro–Wilk normality test. Normally distributed data were analysed by a one-way ANOVA, followed by Tukey’s multiple comparison test (B–E). Non-normally distributed data were analysed column wise by Kruskal–Wallis ranked tests, followed by Dunn’s multiple comparisons test (F). Statistical significance is displayed as \* $P < 0.05$ , \*\* $P < 0.01$ , and \*\*\* $P < 0.001$ .

phospholipid composition clearly separated CD4<sup>+</sup> T cells from a normolipidaemic and hyperlipidaemic environment in a PCA (Figure 5C). However, apart from differences in bis(monoacylglycerol)phosphate (BMP) and phosphatidylserine (PS) levels, hyperlipidaemia was not accompanied by major shifts in phospholipid class composition (Figure 5D). Nonetheless, phosphatidylcholines (PCs) in T cells from HCD-fed mice were found to have longer chains (Figure 5E). Changes in chain length of fatty acids are known to result in reduced membrane fluidity and lipid raft formation and increased membrane thickness.<sup>22,23</sup> We indeed found that HCD-induced cholesterol accumulation reduced membrane fluidity and lipid raft formation (see Supplementary material online, Figure S5C and D). Phospholipid chains are composed of fatty acids, a class of molecules that is highly capable of modulating T cell polarization.<sup>24</sup> Therefore, we analysed the fatty acid composition within phospholipids and focused on arachidonic acid (AA), known to promote pro-inflammatory Th1 and Th17 polarization, and docosahexaenoic acid (DHA), an anti-inflammatory fatty acid that suppresses Th1 and Th17 activation and stimulates Th2 and Treg activation.<sup>25</sup> Interestingly, in line with the enhanced inflammatory T cell responses in HCD-fed mice, we found that a hyperlipidaemic environment increased the ratio of AA to DHA-containing phospholipids in T cells (Figure 5F). Interestingly, transcriptomics analysis of human T cells showed that AA induces many pathways associated with

a Th1-like phenotype in CD4<sup>+</sup> T cells, confirming an important role of AA-induced Th1 skewing (see Supplementary material online, Figure S5E).

To further detail these findings, murine CD4<sup>+</sup> T cells were treated with LDL or VLDL and then subjected to the NSAID ibuprofen, a drug known to decrease AA levels. Only cells treated with VLDL polarized towards a Th1 phenotype, which could be reverted by ibuprofen treatment. These data suggest that VLDL treatment increases the AA/DHA ratio, thereby inducing a Th1-like response.

## Discussion

In the present study, we found that diet-induced hyperlipidaemia in *Ldlr*<sup>-/-</sup> mice increases the effector population of CD4<sup>+</sup> T cells, which produced more IFN- $\gamma$  and exhibited increased surface expression of CXCR3. Both IFN- $\gamma$  and CXCR3 are canonical markers of Th1 cells, considered to be the most pro-atherogenic subset of CD4<sup>+</sup> T cells.<sup>10</sup> Interferon- $\gamma$  promotes atherosclerotic plaque development via several mechanisms, including modulation of macrophage polarization and inhibition of vascular smooth muscle cell proliferation.<sup>10</sup> Likewise, genetic ablation of IFN- $\gamma$  or its receptor reduces atherosclerotic plaque development.<sup>26,27</sup> C-X-C-chemokine receptor 3 is essential for the

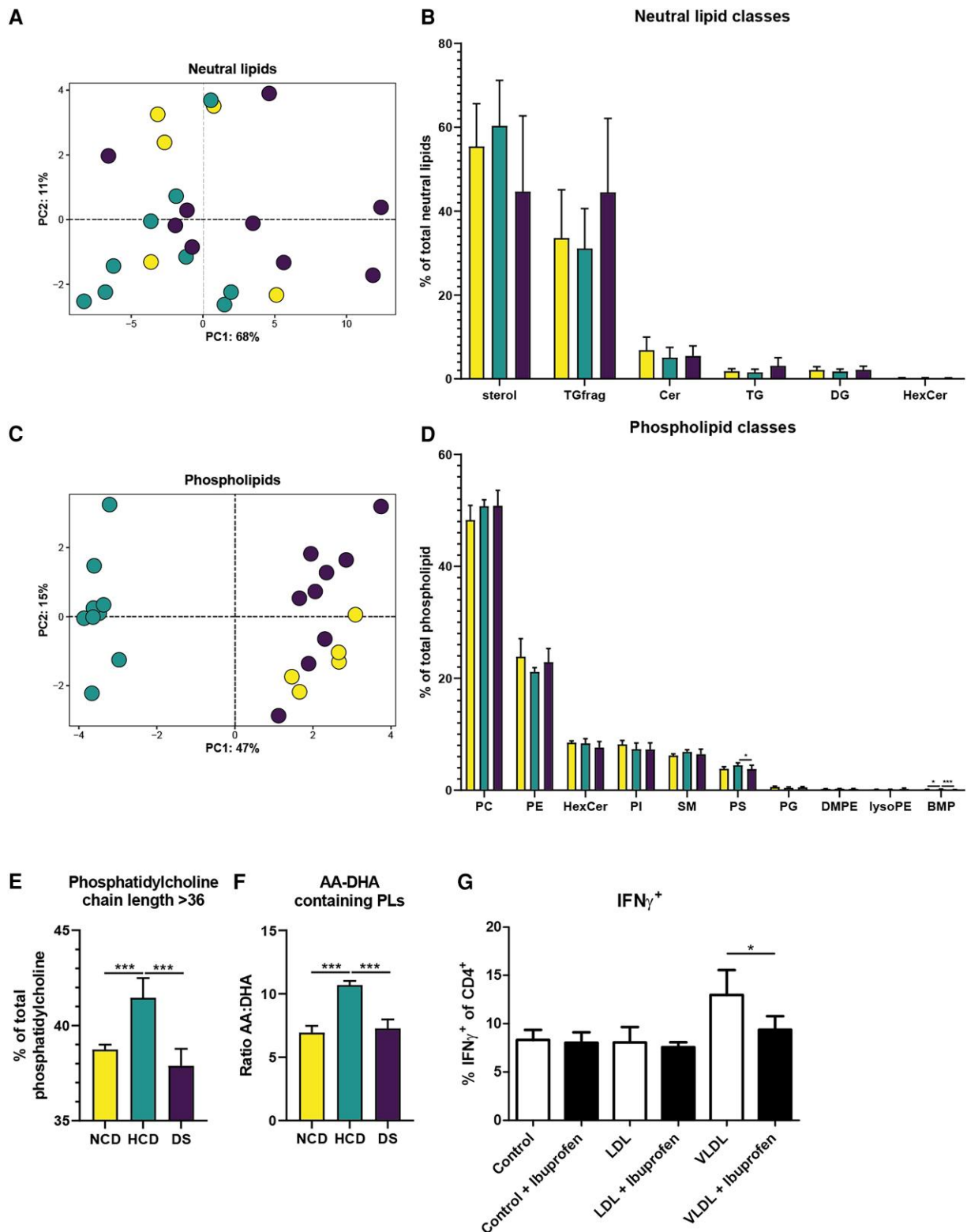


**Figure 5** (A) Principal component analysis of neutral lipids in splenic CD4<sup>+</sup> T cells of NCD ( $n = 5$ ), HCD ( $n = 9$ ), and DS ( $n = 9$ ) fed *Ldlr*<sup>-/-</sup> mice. (B) Relative intensities of neutral lipid classes. (C) PCA of phospholipids in splenic CD4<sup>+</sup> T cells of fed *Ldlr*<sup>-/-</sup> mice. (D) Relative intensities of phospholipid classes. (E) Percentage phosphatidylcholines with a summed fatty acid chain length longer than 36 (F) Ratio of AA to DHA-containing phospholipids. (G) The impact of blocking COX-1/COX-2 with ibuprofen on the frequency of CD3/CD28-activated CD4<sup>+</sup> T cells expressing IFN- $\gamma$ , without treatment, treated with LDL or VLDL ( $n = 6$ ). Data are shown as mean  $\pm$  SD. Statistical significance was analysed by first removing outliers using a ROUT test. Normal distribution of the data was confirmed by a Shapiro–Wilk normality test, followed by a one-way ANOVA with a Tukey’s multiple comparison test. Statistical significance is displayed as \* $P < 0.05$  and \*\*\* $P < 0.001$ .

recruitment of T cells to atherosclerotic plaques via binding to CXCL10. Administration of a CXCR3 antagonist or genetic deletion of CXCR3 in atherosclerosis-prone mice results in reduced atherosclerosis.<sup>28,29</sup>

Depending on the cytokine environment, activation of specific lineage-defining TFs orchestrates the differentiation of naïve CD4<sup>+</sup> T cells into distinct effector subsets.<sup>30</sup> For instance, IL-12 stimulates T cells to produce IFN- $\gamma$ .<sup>31</sup> In turn, autocrine IFN- $\gamma$ -mediated signalling via STAT1 in T cells enhances activation of T-box expressed in T cells (T-bet), the master regulator TF that drives the development of Th1 cells.<sup>18,32</sup> T-bet stimulates the expression of the IL-12 receptor, thereby enhancing the responsiveness of T cells to IL-12.<sup>33</sup> Additionally, T-bet stimulates IFN- $\gamma$  expression in T cells, thereby creating an auto-crine feedback loop in which IFN- $\gamma$  boosts its own production.<sup>18</sup> In agreement with the enhanced presence of canonical Th1 markers, we identified the IFN- $\gamma$  response as the most significantly enriched biological process in T cells from hyperlipidaemic mice. However, transcript levels of *Il12r2b*, encoding the receptor for IL-12, and *Tbet* were not increased in T cells from hyperlipidaemic mice. Therefore, alternative routes must be driving this inflammatory Th1-like phenotype in T cells upon hyperlipidaemia.

In the past few years, several studies have reported that cholesterol accumulation in T cells can have mixed effects on their inflammatory characteristics and their contribution to atherosclerosis, depending on the duration of exposure to hyperlipidaemia and the type of T cell cholesterol accumulation resulting from hyperlipidaemia. Similar to our studies, Magento-García *et al.*<sup>11</sup> showed that prolonged hypercholesterolaemia in mice was accompanied by elevated numbers of CD4<sup>+</sup> effector T cells, and Proto *et al.*<sup>13</sup> found that elevated plasma cholesterol levels in mice with a humanized immune system are associated with an increase of CD4<sup>+</sup> and CD8<sup>+</sup> effector T cells. In contrast, a recent study showed that in advanced atherosclerosis induced by 20 weeks HCD feeding in ApoE<sup>-/-</sup> mice, Th1 cells exhibited decreased IFN- $\gamma$  production, suggesting that T cell functionality is compromised in aged mice, when T cells have accumulated excess cholesterol.<sup>34</sup> Also, inhibition of key mediators in lipid metabolism in T cells resulted in mixed effects on T cell phenotype and/or function. Deficiency of T cell acyl-coenzyme A cholesterol acyltransferase (ACAT) causing an inhibition of cholesterol esterification and an increased membrane cholesterol content resulted in an increase in IFN- $\gamma$ -producing T cells,<sup>35</sup> similar to our study. Deficiency of the ATP-binding cassette (ABC) G1 in T cells induced cholesterol accumulation in the T cell membrane and lipid droplet formation, resulting in an increase in Tregs and a reduction in atherosclerosis.<sup>36</sup> ABCA1 deficiency reduced TCR signalling and the formation of effector memory cells. However, deficiency of T cell ABCA1 resulted in increased expression of T cell ABCG1, resulting in a decrease in membrane lipid rafts.<sup>37</sup> Combined deficiency of ABCA1 and ABCG1 in T cells induced cholesterol and cholesterol ester accumulation, increased membrane cholesterol content, and induced T cell membrane stiffening. *Abca1/Abcg1/Ldlr*<sup>-/-</sup> mice displayed enhanced T cell activation, with more effector memory and central memory populations in their CD4<sup>+</sup> and CD8<sup>+</sup> T cell subsets. Surprisingly, the total number of T cells had decreased, which was due to increased T cell apoptosis and senescence, especially in middle aged mice, which also displayed a reduction in atherosclerosis.<sup>38</sup>

Interestingly, Tregs can acquire Th1 and follicular helper T (Tfh) like inflammatory properties during atherogenesis and CVD, which is thought to be induced by hyperlipidaemia. Regulatory T cells from ApoE<sup>-/-</sup> mice that were fed a Western-type diet for 20 weeks experienced a phenotypic switch towards Th1- and Tfh-like cells, expressing IFN- $\gamma$ , bcl6, and IL-21. These effects could be reverted by injections with ApoA1, which induced T cell cholesterol efflux.<sup>39</sup> Also, ApoB100 reactive T cells of hyperlipidaemic ApoE<sup>-/-</sup> mice that showed characteristics of Th1/Th17 and Tfh cells, displayed a residual Treg transcriptome, suggesting that hyperlipidaemia turns Tregs into

pro-atherogenic T cell phenotypes.<sup>40,41</sup> A similar phenomenon could be observed in CVD patients where ApoB-specific Tregs switch to a more memory-like phenotype.<sup>41–43</sup> In our data, we could not find a residual Treg transcriptome in our Th1-like cells. However, we did find an increased number of splenic Tregs. The lack of Treg to memory-like switching might be due to shorter exposure to hyperlipidaemia in our study, and it may very well be that we see an increase of dysfunctional Tregs in our study.

Hyperlipidaemia-induced alterations of intracellular metabolic programs might affect the inflammatory capacities of T cells, as was previously reported for macrophages.<sup>44</sup> Emerging evidence demonstrates that rewiring of intracellular metabolism is tightly intertwined with T cell activation and effector functions.<sup>19,20</sup> For instance, high rates of aerobic glycolysis are required for the production of IFN- $\gamma$  by T cells.<sup>45</sup> However, abundance of glycolysis metabolites or intermediates of other metabolic pathways associated with immune cell activation, such as the PPP, were not increased in T cells upon hyperlipidaemia. Nevertheless, we detected an enrichment of several amino acids in T cells from hyperlipidaemic mice. In addition to protein synthesis, amino acids are crucial for many processes during T cell activation, including nucleotide synthesis, maintaining redox balances, feeding energy-producing pathways, and supplying intermediates for post-translational and epigenetic modifications.<sup>46</sup> For instance, methionine, found to be enriched in T cells upon hyperlipidaemia, can be converted into the universal methyl donor S-adenosylmethionine (SAM) that is used by activated T cells for methylation reactions that are essential for their activation.<sup>47</sup> The frequency of IFN- $\gamma$ -producing CD4<sup>+</sup> T cells was reported to be dependent on the supply of extracellular methionine, indicating that methionine availability is rate limiting for Th1 activation.<sup>47</sup> In addition to amino acids, we found a significant increase of creatine in T cells from hyperlipidaemic mice. This nitrogenous organic acid was recently found to be essential for CD8<sup>+</sup> T cell antitumor immunity, as creatine uptake deficiency in mice diminishes the production of effector cytokines, including IFN- $\gamma$ , and accelerates tumour growth.<sup>48</sup> Altogether, elevated intracellular levels of amino acids or metabolites such as creatine in T cells could support their inflammatory capacities induced by hyperlipidaemia. However, it remains to be further investigated whether these increases are the cause or consequence of the enhanced inflammatory T cell phenotype observed in hyperlipidaemic mice. In this respect, the results of the study of Gaddis *et al.* are interesting. When ApoE<sup>-/-</sup> mice were fed a cholesterol-rich diet for a prolonged period of time (20 weeks), naïve T cells could not be activated anymore by  $\alpha$ CD3/ $\alpha$ CD28 *in vitro*, failed to take up glucose, and displayed decreased glycolytic capacity and reserve,<sup>34</sup> suggesting that prolonged exposure to hyperlipidaemia renders T cells metabolically inactive.

Our transcriptomic data point towards dysregulated cholesterol homeostasis of T cells from hyperlipidaemic mice, as illustrated by enhanced expression of both liver x receptor (LXR) and sterol regulatory element-binding protein (SREBP) target genes. Evidence of studies disturbing LXR or SREBP signalling pathways indicate that intracellular cholesterol promotes CD8<sup>+</sup> T cell proliferation and IFN- $\gamma$  production.<sup>21,49</sup> Moreover, enrichment of cholesterol in the membranes of CD4<sup>+</sup> T cells was reported to promote Th1 differentiation and IFN- $\gamma$  secretion.<sup>50</sup> In line with these reports, we detected slightly elevated intracellular cholesterol levels in T cells from hyperlipidaemic mice. Therefore, perturbations within the systemic cholesterol environment, such as during hyperlipidaemia, may alter the intracellular cholesterol milieu within T cells, thereby favouring differentiation of T cells towards an increased inflammatory state.

A large body of evidence from numerous clinical and genetic studies indisputably demonstrates a causal relationship between elevated LDL-C levels and atherosclerotic CVD.<sup>51</sup> Moreover, increased levels of circulating effector memory CD4<sup>+</sup> T cells correlate with LDL-C levels in humans.<sup>12</sup> Interestingly, our study showed that exposure of T



cells to LDL had no effect on the transcriptomic profile of these cells *in vitro*. In contrast, incubation with VLDL resulted in the deregulation of hundreds of genes in murine T cells. Furthermore, exposure to VLDL, but not to LDL, stimulated cytokine production of IFN- $\gamma$  in murine T cells and TNF- $\alpha$  in human T cells, both implicated in the progression of atherosclerosis.<sup>52</sup>

Very low-density lipoprotein was previously found to promote pro-inflammatory responses in macrophages via up-regulation of intracellular C16:0 ceramides levels.<sup>15</sup> Therefore, elevated plasma levels of VLDL upon hyperlipidaemia might deregulate lipid composition within T cells, thereby evoking inflammatory responses. We found that PCs in T cells from HCD-fed mice were composed of longer fatty acid chains. Further research is needed to investigate the influence of PC fatty acid chain length on inflammatory responses in T cells. Nevertheless, we found that the ratio of AA to DHA in phospholipids was increased in T cells from HCD-fed mice. Arachidonic acid was previously found to promote the differentiation of T cells towards Th1, whereas DHA disturbs Th1 differentiation.<sup>25</sup> Therefore, an unbalanced AA to DHA ratio in T cells might contribute to their increased inflammatory responses upon hyperlipidaemia.

Altogether, in this study, we show that hyperlipidaemia induces a pro-inflammatory Th1-like response in CD4<sup>+</sup> T cells and found that VLDL, but not LDL, is responsible for this phenotype.

## Lead author biography



Bram van Os received his bachelor's and master's degrees in Biopharmaceutical Sciences at Leiden University. Currently, he is pursuing his PhD at the Amsterdam UMC under the supervision of Prof. Esther Lutgens, MD, PhD. During his master he developed an interest in the immune system and its role in atherosclerosis. His main interest is T cell biology in the context of atherosclerosis and hyperlipidaemia.

## Data availability

RNA-seq data are deposited in the Gene Expression Omnibus (GEO) database under accession numbers GSE196970 and GSE196971.

## Supplementary material

Supplementary material is available at *European Heart Journal Open* online.

## Acknowledgements

We thank Tom T.P. Seijkens, Kikkie Poels, Myrthe E. Reiche, and Pascal J. H. Kusters for their help and support.

## Funding

This work was supported by the Netherlands CardioVascular Research Initiative: the Dutch Heart Foundation, Dutch Federation of University Medical Centres, the Netherlands Organization for Health Research and Development and the Royal Netherlands Academy of Sciences for the GENIUS-II project 'Generating the best evidence-based pharmaceutical targets for atherosclerosis' (CVON2017-20 to E.L.). This study was supported by the Deutsche Forschungsgemeinschaft (CRC 1123 to D.A., E.L., and C.W., DFG Einzelförderung 451372580 to D.A.). This study was also

supported by the German Centre for Cardiovascular Research (DZHK) (Women Scientist grant to D.A. and Translational Research Project grant to E.L., D.A., and C.W.) and the European Research Council (ERC Consolidator Grant to E.L., ERC Advanced Grant to C.W.). C.W. is a Van de Laar professor of atherosclerosis.

**Conflict of interest:** None declared.

## References

- Virani SS, Alonso A, Aparicio HJ, Benjamin EJ, Bittencourt MS, Callaway CW, Carson AP, Chamberlain AM, Cheng S, Delling FN, Elkind MSV, Evenson KR, Ferguson JF, Gupta DK, Khan SS, Kissela BM, Knutson KL, Lee CD, Lewis TT, Liu J, Loop MS, Lutsey PL, Ma J, Mackey J, Martin SS, Matchar DB, Mussolino ME, Navaneethan SD, Perak AM, Roth GA, Samad Z, Satou GM, Schroeder EB, Shah SH, Shay CM, Stokes A, VanWagner LB, Wang N-Y, Tsao CW. Heart disease and stroke statistics-2021 update: a report from the American Heart Association. *Circulation* 2021;**143**:e254–e743.
- Jukema JW, Cannon CP, de Craen AJM, Westendorp RGJ, Trompet S. The controversies of statin therapy: weighing the evidence. *J Am Coll Cardiol* 2012;**60**: 875–881.
- Aday AW, Ridker PM. Targeting residual inflammatory risk: a shifting paradigm for atherosclerotic disease. *Front Cardiovasc Med* 2019;**6**:16.
- Ridker PM, Everett BM, Thuren T, MacFadyen JG, Chang WH, Ballantyne C, Fonseca F, Nicolau J, Koenig W, Anker SD, Kastelein JJP, Cornel JH, Pais P, Pella D, Genest J, Cifkova R, Lorenzatti A, Forster T, Kobalava Z, Vida-Simiti L, Flather M, Shimokawa H, Ogawa H, Dellborg M, Rossi PRF, Troquay RPT, Libby P, Glynn RJ. Antiinflammatory therapy with canakinumab for atherosclerotic disease. *N Engl J Med* 2017;**377**:1119–1131.
- Nidorf SM, Fiolet ATL, Mosterd A, Eikelboom JW, Schut A, Opstal TSJ, The SHK, Xu X-F, Ireland MA, Lenderink T, Latchem D, Hoogslag P, Jerzewski A, Nierop P, Whelan A, Hendriks R, Swart H, Schaap J, Kuijper AFM, van Hesse MWJ, Saklani P, Tan I, Thompson AG, Morton A, Judkins C, Bax WA, Dirksen M, Alings M, Hankey GJ, Budgeon CA, Tijssen JGP, Cornel JH, Thompson PL. Colchicine in patients with chronic coronary disease. *N Engl J Med* 2020;**383**:1838–1847.
- Ridker PM, Everett BM, Pradhan A, MacFadyen JG, Solomon DH, Zaharris E, Mam V, Hasan A, Rosenberg Y, Iturriga E, Gupta M, Tsigoulis M, Verma S, Clearfield M, Libby P, Goldhaber SZ, Seagle R, Ofori C, Saklayen M, Butman S, Singh N, Le MM, Bertrand O, Johnston J, Paynter NP, Glynn RJ. Low-Dose methotrexate for the prevention of atherosclerotic events. *N Engl J Med* 2019;**380**:752–762.
- Lutgens E, Atzler D, Döring Y, Duchene J, Steffens S, Weber C. Immunotherapy for cardiovascular disease. *Eur Heart J* 2019;**40**:3937–3946.
- Fernandez DM, Rahman AH, Fernandez NF, Chudnovskiy A, Amir E-AD, Amadori L, Khan NS, Wong CK, Shamailova R, Hill CA, Wang Z, Remark R, Li JR, Pina C, Faries C, Awad AJ, Moss N, Björkegren JLM, Kim-Schulze S, Gnjatich S, Ma'ayan A, Mocco J, Faries P, Merad M, Giannarelli C. Single-cell immune landscape of human atherosclerotic plaques. *Nat Med* 2019;**25**:1576–1588.
- Depuydt MAC, Prange KHM, Slenders L, Örd T, Elbersen D, Boltjes A, de Jager SCA, Asselbergs FW, de Borst GJ, Aavik E, Lönnberg T, Lutgens E, Glass CK, den Ruijter HM, Kaikkonen MU, Bot I, Slütter B, van der Laan SW, Yla-Herttuala S, Mokry M, Kuiper J, de Winther MPJ, Pasterkamp G. Microanatomy of the human atherosclerotic plaque by single-cell transcriptomics. *Circ Res* 2020;**127**:1437–1455.
- Saigusa R, Winkels H, Ley K. T cell subsets and functions in atherosclerosis. *Nat Rev Cardiol* 2020;**17**:387–401.
- Maganto-García E, Tarrío ML, Grabié N, Bu D, Lichtman AH. Dynamic changes in regulatory T cells are linked to levels of diet-induced hypercholesterolemia. *Circulation* 2011;**124**:185–195.
- Ammirati E, Cianflone D, Vecchio V, Banfi M, Vermi AC, De MM, Grigore L, Pellegatta F, Pirillo A, Garlaschelli K, Manfredi AA, Catapano AL, Maseri A, Palini AG, Norata GD. Effector memory T cells are associated with atherosclerosis in humans and animal models. *J Am Heart Assoc* 2012;**1**:27–41.
- Proto JD, Doran AC, Subramanian M, Wang H, Zhang M, Sozen E, Rymond CC, Kuriakose G, D'Agati V, Winchester R, Sykes M, Yang Y-G, Tabas I. Hypercholesterolemia induces T cell expansion in humanized immune mice. *J Clin Invest* 2018;**128**:2370–2375.
- Lillis AP, Mikhailenko I, Strickland DK. Beyond endocytosis: LRP function in cell migration, proliferation and vascular permeability. *J Thromb Haemost* 2005;**3**:1884–1893.
- Shin KC, Hwang I, Choe SS, Park J, Ji Y, Kim JI, Lee GY, Choi SH, Ching J, Kovalik J-P, Kim JB. Macrophage VLDLR mediates obesity-induced insulin resistance with adipose tissue inflammation. *Nat Commun* 2017;**8**:1087.
- Platanias LC. Mechanisms of type-I- and type-II-interferon-mediated signalling. *Nat Rev Immunol* 2005;**5**:375–386.
- Platanitis E, Demiroz D, Schneller A, Fischer K, Capelle C, Hartl M, Gossenreiter T, Müller M, Novatchkova M, Decker T. A molecular switch from STAT2-IRF9 to ISGF3 underlies interferon-induced gene transcription. *Nat Commun* 2019;**10**:2921.

18. Lighvani AA, Frucht DM, Jankovic D, Yamane H, Aliberti J, Hissong BD, Nguyen BV, Gadina M, Sher A, Paul WE, O'Shea JJ. T-bet is rapidly induced by interferon-gamma in lymphoid and myeloid cells. *Proc Natl Acad Sci U S A* 2001;**98**:15137–15142.
19. Geltink RIK, Kyle RL, Pearce EL. Unraveling the Complex interplay between T cell metabolism and function. *Annu Rev Immunol* 2018;**36**:461–488.
20. Chapman NM, Boothby MR, Chi H. Metabolic coordination of T cell quiescence and activation. *Nat Rev Immunol* 2020;**20**:55–70.
21. Bensinger SJ, Bradley MN, Joseph SB, Zelcer N, Janssen EM, Hausner MA, Shih R, Parks JS, Edwards PA, Jamieson BD, Tontonoz P. LXR Signaling couples sterol metabolism to proliferation in the acquired immune response. *Cell* 2008;**134**:97–111.
22. Fan Y-Y, Fuentes NR, Hou TY, Barhouni R, Li XC, Deutz NEP, Engelen MPKJ, McMurray DN, Chapkin RS. Remodelling of primary human CD4+ T cell plasma membrane order by n-3 PUFA. *Br J Nutr* 2018;**119**:163–175.
23. Al-Aghbar MA, Jainarayanan AK, Dustin ML, Roffler SR. The interplay between membrane topology and mechanical forces in regulating T cell receptor activity. *Commun Biol* 2022;**5**:40.
24. Reilly NA, Lutgens E, Kuiper J, Heijmans BT, Wouter Jukema J. Effects of fatty acids on T cell function: role in atherosclerosis. *Nat Rev Cardiol* 2021;**18**:824–837.
25. Bi X, Li F, Liu S, Jin Y, Zhang X, Yang T, Dai Y, Li X, Zhao AZ.  $\omega$ -3 polyunsaturated fatty acids ameliorate type 1 diabetes and autoimmunity. *J Clin Invest* 2017;**127**:1757–1771.
26. Gupta S, Pablo AM, Jiang XC, Wang N, Tall AR, Schindler C. IFN- $\gamma$  potentiates atherosclerosis in ApoE knock-out mice. *J Clin Invest* 1997;**99**:2752–2761.
27. Buono C, Come CE, Stavrakis G, Maguire GF, Connelly PW, Lichtman AH. Influence of interferon- $\gamma$  on the extent and phenotype of diet-induced atherosclerosis in the LDLR-deficient mouse. *Arterioscler Thromb Vasc Biol* 2003;**23**:454–460.
28. Veillard NR, Steffens S, Pelli G, Lu B, Kwak BR, Gerard C, Charo IF, Mach F. Differential influence of chemokine receptors CCR2 and CXCR3 in development of atherosclerosis in vivo. *Circulation* 2005;**112**:870–878.
29. van Wanrooij EJA, de Jager SCA, van Es T, de Vos P, Birch HL, Owen DA, Watson RJ, Biessen EAL, Chapman GA, van Berkel TJC, Kuiper J. CXCR3 Antagonist NBI-74330 attenuates atherosclerotic plaque formation in LDL receptor-deficient mice. *Arterioscler Thromb Vasc Biol* 2008;**28**:251–257.
30. Zhu J, Yamane H, Paul WE. Differentiation of effector CD4 T cell populations (\*). *Annu Rev Immunol* 2010;**28**:445–489.
31. Hsieh CS, Macatonia SE, Tripp CS, Wolf SF, O'Garra A, Murphy KM. Development of TH1 CD4+ T cells through IL-12 produced by Listeria-induced macrophages. *Science* 1993;**260**:547–549.
32. Szabo SJ, Kim ST, Costa GL, Zhang X, Fathman CG, Glimcher LH. Pillars article: a novel transcription factor, T-bet, directs Th1 lineage commitment. *J Immunol* 2015;**194**:2961–2975.
33. Afkarian M, Sedy JR, Yang J, Jacobson NG, Cereb N, Yang SY, Murphy TL, Murphy KM. T-bet is a STAT1-induced regulator of IL-12R expression in naïve CD4+ T cells. *Nat Immunol* 2002;**3**:549–557.
34. Gaddis DE, Padgett LE, Wu R, Nguyen A, McSkimming C, Dinh HQ, Araujo DJ, Taylor AM, McNamara CA, Hedrick CC. Atherosclerosis impairs naïve CD4 T-cell responses via disruption of glycolysis. *Arterioscler Thromb Vasc Biol* 2021;**41**:2387–2398.
35. Yang W, Bai Y, Xiong Y, Zhang J, Chen S, Zheng X, Meng X, Li L, Wang J, Xu C, Yan C, Wang L, Chang CCY, Chang T-Y, Zhang T, Zhou P, Song B-L, Liu W, Sun S, Liu X, Li B, Xu C. Potentiating the antitumor response of CD8(+) T cells by modulating cholesterol metabolism. *Nature* 2016;**531**:651–655.
36. Cheng H-Y, Gaddis DE, Wu R, McSkimming C, Haynes LD, Taylor AM, McNamara CA, Sorci-Thomas M, Hedrick CC. Loss of ABCG1 influences regulatory T cell differentiation and atherosclerosis. *J Clin Invest* 2016;**126**:3236–3246.
37. Zhao Y, Zhang L, Liu L, Zhou X, Ding F, Yang Y, Du S, Wang H, Van EM, Wang J. Specific loss of ABCA1 (ATP-binding cassette transporter A1) suppresses TCR (T-cell receptor) signaling and provides protection against atherosclerosis. *Arterioscler Thromb Vasc Biol* 2022;**42**:e311–e326.
38. Baziotti V, La RA, Maassen S, Bianchi F, de Boer R, Halmos B, Dabral D, Guilbaud E, Flohr-Svendsen A, Groenen AG, Marmolejo-Garza A, Koster MH, Kloosterhuis NJ, Havinga R, Pranger AT, Langelaar-Makkinje M, de Bruin A, van de Sluis B, Kohan AB, Yvan-Charvet L, van den Bogaart G, Westerterp M. T cell cholesterol efflux suppresses apoptosis and senescence and increases atherosclerosis in middle aged mice. *Nat Commun* 2022;**13**:3799.
39. Gaddis DE, Padgett LE, Wu R, McSkimming C, Romines V, Taylor AM, McNamara CA, Kronenberg M, Crotty S, Thomas MJ, Sorci-Thomas MG, Hedrick CC. Apolipoprotein AI prevents regulatory to follicular helper T cell switching during atherosclerosis. *Nat Commun* 2018;**9**:1095.
40. Schoenborn JR, Wilson CB. Regulation of interferon- $\gamma$  during innate and adaptive immune responses. *Adv Immunol* 2007;**96**:41–101.
41. Wolf D, Gerhardt T, Winkels H, Michel NA, Pramod AB, Ghosheh Y, Brunel S, Buscher K, Miller J, McArdle S, Baas L, Kobiyama K, Vassallo M, Ehinger E, Dileepan T, Ali A, Schell M, Mikulski Z, Sidler D, Kimura T, Sheng X, Horstmann H, Hansen S, Mitre LS, Stachon P, Hilgendorf I, Gaddis DE, Hedrick C, Benedict CA, Peters B, Zirlik A, Sette A, Ley K. Pathogenic autoimmunity in atherosclerosis evolves from initially protective apolipoprotein B(100)-reactive CD4(+) T-regulatory cells. *Circulation* 2020;**142**:1279–1293.
42. Kimura T, Kobiyama K, Winkels H, Tse K, Miller J, Vassallo M, Wolf D, Ryden C, Orecchioni M, Dileepan T, Jenkins MK, James EA, Kwok WW, Hanna DB, Kaplan RC, Strickler HD, Durkin HG, Kassaye SG, Karim R, Tien PC, Landay AL, Gange SJ, Sidney J, Sette A, Ley K. Regulatory CD4(+) T cells recognize major histocompatibility Complex class II molecule-restricted peptide epitopes of apolipoprotein B. *Circulation* 2018;**138**:1130–1143.
43. Saigusa R, Roy P, Freuchet A, Gulati R, Ghosheh Y, Suthahar SSA, Durant CP, Hanna DB, Kiesses WB, Orecchioni M, Wen L, Wu R, Kuniholm MH, Landay AL, Anastos K, Tien PC, Gange SJ, Kassaye S, Vallejo J, Hedrick CC, Kwok WW, Sette A, Hodis HN, Kaplan RC, Ley K. Single cell transcriptomics and TCR reconstruction reveal CD4 T cell response to MHC-II-restricted APOB epitope in human cardiovascular disease. *Nat Cardiovasc Res* 2022;**1**:462–475.
44. Baardman J, Verberk SGS, Prange KHM, van Weeghel M, van der Velden S, Ryan DG, Wüst RC, Neele AE, Speijer D, Denis SW, Witte ME, Houtkooper RH, O'Neill LA, Knatko EV, Dinkova-Kostova AT, Lutgens E, de Winther MPJ, van den Bossche J. A defective pentose phosphate pathway reduces inflammatory macrophage responses during hypercholesterolemia. *Cell Rep* 2018;**25**:2044–2052.e5.
45. Siska PJ, Rathmell JC. Metabolic signaling drives IFN- $\gamma$ . *Cell Metab* 2016;**24**:651–652.
46. Kelly B, Pearce EL. Amino assets: how amino acids support immunity. *Cell Metab* 2020;**32**:154–175.
47. Sinclair L V, Howden AJ, Brenes A, Spinelli L, Hukelmann JL, Macintyre AN, Liu X, Thomson S, Taylor PM, Rathmell JC, Locasale JW, Lamond AI, Cantrell DA. Antigen receptor control of methionine metabolism in T cells. *Elife* 2019;**8**:e44210.
48. Di Biase S, Ma X, Wang X, Yu J, Wang Y-C, Smith DJ, Zhou Y, Li Z, Kim YJ, Clarke N, To A, Yang L. Creatine uptake regulates CD8 T cell antitumor immunity. *J Exp Med* 2019;**216**:2869–2882.
49. Kidani Y, Elsaesser H, Hock MB, Vergnes L, Williams KJ, Argus JP, Marbois BN, Komisopoulou E, Wilson EB, Osborne TF, Graeber TG, Reue K, Brooks DG, Bensinger SJ. Sterol regulatory element-binding proteins are essential for the metabolic programming of regulatory T cells and adaptive immunity. *Nat Immunol* 2013;**14**:489–499.
50. Surlis J, Nazarov-Stoica C, Kehl M, Olsen C, Casares S, Brumeanu T-D. Increased membrane cholesterol in lymphocytes diverts T-cells toward an inflammatory response. *PLoS One* 2012;**7**:e38733.
51. Ference BA, Ginsberg HN, Graham I, Ray KK, Packard CJ, Bruckert E, Hegele RA, Krauss RM, Raal FJ, Schunkert H, Watts GF, Borén J, Fazio S, Horton JD, Masana L, Nicholls SJ, Nordestgaard BG, van de Sluis B, Taskiran MR, Tokgözoğlu L, Landmesser U, Laufs U, Wiklund O, Stock JK, Chapman MJ, Catapano AL. Low-density lipoproteins cause atherosclerotic cardiovascular disease. 1. Evidence from genetic, epidemiologic, and clinical studies. A consensus statement from the European Atherosclerosis Society Consensus Panel. *Eur Heart J* 2017;**38**:2459–2472.
52. Tousoulis D, Oikonomou E, Economou EK, Crea F, Kaski JC. Inflammatory cytokines in atherosclerosis: current therapeutic approaches. *Eur Heart J* 2016;**37**:1723–1732.
53. Fedoseienko A, Wijers J, Wolters JC, Dekker D, Smit M, Huijman N, Kloosterhuis N, Klug H, Schepers A, Willems van Dijk K, Levels JHM, Billadeau DD, Hofker MH, van Deursen J, Westerterp M, Burstein E, Kuivenhoven JA, van de Sluis B. The COMMD family regulates plasma LDL levels and attenuates atherosclerosis through stabilizing the CCC Complex in endosomal LDLR trafficking. *Circ Res* 2018;**122**:1648–1660.
54. Dobin A, Davis CA, Schlesinger F, Drenkow J, Zaleski C, Jha S, Batut P, Chaisson M, Gingeras TR. STAR: ultrafast universal RNA-seq aligner. *Bioinformatics* 2013;**29**:15–21.
55. Li H, Handsaker B, Wysoker A, Fennell T, Ruan J, Homer N, Marth G, Abecasis G, Durbin R. The sequence alignment/map format and SAMtools. *Bioinformatics* 2009;**25**:2078–2079.
56. Love MI, Huber W, Anders S. Moderated estimation of fold change and dispersion for RNA-seq data with DESeq2. *Genome Biol* 2014;**15**:550.
57. Yu G, Wang L-G, Han Y, He Q-Y. ClusterProfiler: an R package for comparing biological themes among gene clusters. *OMICS* 2012;**16**:284–287.
58. Zhou Y, Zhou B, Pache L, Chang M, Khodabakhshi AH, Tanaseichuk O, Benner C, Chanda SK. Metascape provides a biologist-oriented resource for the analysis of systems-level datasets. *Nat Commun* 2019;**10**:1523.
59. Zambelli F, Pesole G, Pavesi G. Pscan: finding over-represented transcription factor binding site motifs in sequences from co-regulated or co-expressed genes. *Nucleic Acids Res* 2009;**37**:W247–W252.
60. Wickham H. Ggplot2. *Wiley Interdiscip Rev Comput Stat* 2011;**3**:180–185.
61. Kolde R. Pretty heatmaps (version 1.0.12). Google Sch 2019.
62. Bligh EG, Dyer WJ. A rapid method of total lipid extraction and purification. *Can J Biochem Physiol* 1959;**37**:911–917.
63. Smith CA, Want EJ, O'Maille G, Abagyan R, Siuzdak G. XCMS: processing mass spectrometry data for metabolite profiling using nonlinear peak alignment, matching, and identification. *Anal Chem* 2006;**78**:779–787.